Novel ultrasonic motor using torsional/ longitudinal vibration

S. Bhargava[1] and D.W. Greve[1,2]
[1]Department of Electrical and Computer Engineering
Carnegie Mellon University, Pittsburgh, PA
[2]National Energy and Technology Laboratory
Pittsburgh, PA

I.J. Oppenheim
Department of Civil and Environmental Engineering
Carnegie Mellon University, Pittsburgh, PA
National Energy and Technology Laboratory
Pittsburgh, PA

***Abstract*—Longitudinal-torsional mode converters have greatly simplified the structure of ultrasonic motors using a combined torsional/ longitudinal vibration, making miniaturization more practical. A previous design of this type of motor used a multi-layer piezoelectric actuator. In this paper, we report on the performance of motors using wafer-type actuators. This motor design requires a reduced volume of piezoelectric material.**

Keywords- ultrasonic motor, piezoelectric, wafer, torsional, longitudinal.

I. INTRODUCTION

Hybrid transducer ultrasonic motors utilizing torsional and longitudinal vibrations have been investigated recently by several groups [1-3]. The advantages of motors of this type include high output torque compared to travelling-wave motors. The required torsional and longitudinal vibrations can be created by two independent piezoelectric transducers or, more simply, by using a torsional-longitudinal mode converter. The spiral mode converter recently investigated by Wajchman *et al.* [3] is of particular interest because of its potential for scaling to microscale motors. That motor was actuated using a multi-layer piezoelectric stack; in this paper we report an alternate scheme in which wafer-type transducers are used as the actuators.

The use of a wafer-type actuator is suggested by the nature of the longitudinal modes excited in the spiral. The longitudinal modes have a uniform displacement in the direction of the axis, similar to the S0 mode excited by the wafer transducer in a plate [4]. When a wafer transducer is placed on one side of a plate both A0 and S0 modes are excited to some degree; however symmetric excitation of a pair of wafers yields a pure S0 mode.

II. COMPARISON OF ACTUATORS

Figure 1 shows the wafer-actuated mode converter considered here along with the multi-layer piezoelectric actuator (MLPA) design. We will first compare the characteristics of the wafer-actuated design with a multi-layer piezoelectric actuator fabricated using the same piezoelectric material. For a rough indication of the effectiveness of actuation, we compare the static displacement resulting from equal applied voltages. We also compare the terminal capacitance.

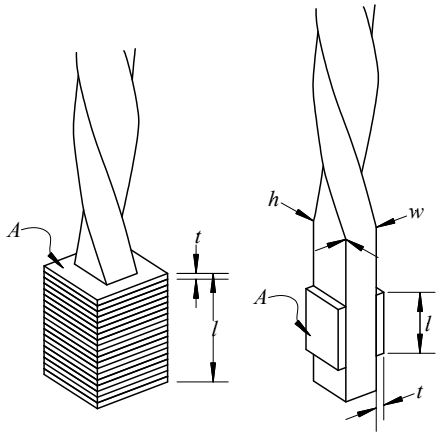

Figure 1. Wafer-actuated spiral mode converter.

We assume that the piezoelectric material is poled in a direction normal to the metallization. For the MLPA, the static displacement Δz for an applied voltage V is

$$\Delta z = d_{31}\frac{V}{t}l \tag{1}$$

where the stack height $l = Nt$, and N is the number of layers in the stack. For the wafer actuator, we have

$$\Delta z = d_{33}\frac{V}{t}l \cdot \tag{2}$$

For terminal capacitance, we obtain for the MLPA

$$C = \frac{\varepsilon_{33}A}{t}\cdot N \tag{3}$$

and for the wafer transducer

$$C = 2\frac{\varepsilon_{33}A}{t} \cdot \tag{4}$$

Comparing these results, we see that the MLPA transducer has somewhat larger static displacement because $|d_{31}| > d_{33}$;

however the input capacitance is much larger as $N >> 2$. We expect the wafer transducer to require higher drive voltages but much lower reactive current.

III. Motor Fabrication and Measurements

Dimensional parameters for the motors considered here are in Table I. Several motors with differing aspect ratios for the spiral were constructed from plexiglas and actuated by wafers of PZT-7A material 6.5 × 9.5 × 0.64 mm in size. Plexiglas spirals were made by twisting plexiglas that had been heated to its softening point. These motors were tested by clamping at the bottom in a steel vise.

Clamping the spiral at the bottom introduces some uncertainty about the boundary condition, complicating comparison with the predictions of finite element simulations. One motor with a symmetric double-spiral was fabricated from aluminum. This motor was clamped on part of the spiral using small pieces of plastic foam between the jaws of the vise and the motor. In this case, the piezoelectric wafers were 0.029" thick of material with $\varepsilon \sim 3800\varepsilon_0$. In all cases, the spiral was in the clockwise direction looking down on the spiral.

TABLE I. DIMENSIONS OF MOTOR STATORS.

motor	material	*w* (mm)	*h* (mm)	*L* (mm)	*h/w*	*N* (rev)
3	PMMA	3.0	6.1	47.3	2.03	1.75
4	PMMA	3.0	4.8	48.6	1.60	2
5	PMMA	3.0	7.5	46.2	2.50	2
6	Al	3.2	6.6	50.4	2.06	2

A circular brass rotor with a 0.91 mm diameter axle was used as the rotor. The axle fit into a 1.02 mm diameter hole drilled into the top of the spiral. In the experiments reported here, the rotor had a total mass of 2.6 gm (PMMA motors) or 6.5 gm (double spiral motor). The motor was driven by an HP-3314A function generator followed by a Piezo Systems EPA-104 amplifier. Rotation was sensed using an infrared LED and phototransistor connected to an NI PCI-6110 DAQ board that detected transitions and converted the transitions into a rotational frequency. Admittance was measured as a function of frequency using an Agilent 4192A impedance analyzer.

IV. Plexiglas Motors

For these motors, admittance at the driving terminals was measured as a function of frequency from 10-200 kHz and input frequencies resulting in rotation were recorded. Figure 2 and Figure 3 show the results obtained for motor 3 with a driving voltage of 150 V peak. This figure plots the measured admittance magnitude divided by frequency ($|Y|/\omega$) and also the admittance phase angle. The phase angle is close to 90 degrees (corresponding to a pure capacitance) except where significant energy is absorbed by the motor.

For motor 3, rotation is observed at many different frequencies over the frequency range investigated. Frequencies corresponding to rotation are indicated in Figure 2 and Figure 3 where CW rotation is indicated by a square point and CCW rotation by a circle. Comparison between the frequencies of rotation and frequencies corresponding to large in-phase currents shows that rotation is sometimes, but not always associated with large in-phase currents. Simulations reported elsewhere [5] suggest that rotation can result from torsional modes alone, and that these modes do not result in strong resonance structure in the admittance measurements.

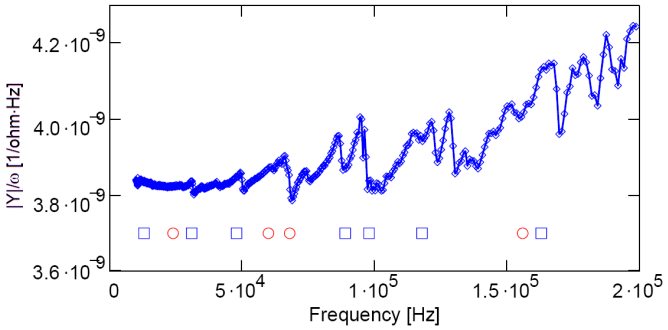

Figure 2. Normalized admittance magnitude for motor 3. The points indicate frequencies of rotation (square = CW, circle = CCW).

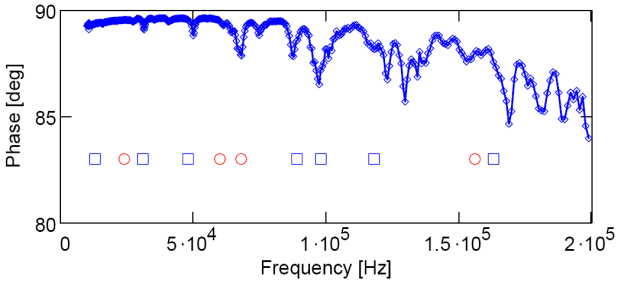

Figure 3. Normalized admittance phase for motor 3. The points indicate frequencies of rotation (square = CW, circle = CCW).

Limited experiments were performed on motor 4 because of permanent changes due to overheating. Figure 4 shows admittance measurements and observed rotation frequencies for motor 5. In this motor, considerably fewer frequencies resulted in rotation.

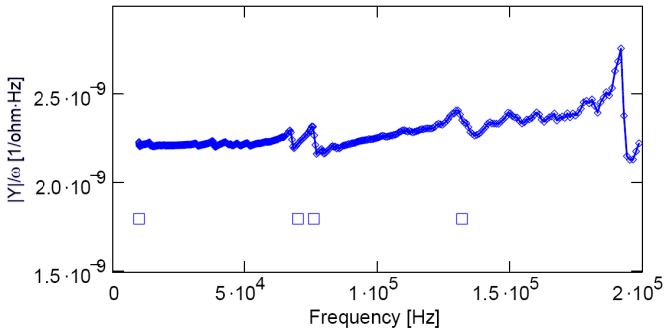

Figure 4. Normalized admittance magnitude for motor 5. The points indicate frequencies of rotation (square = CW, circle = CCW).

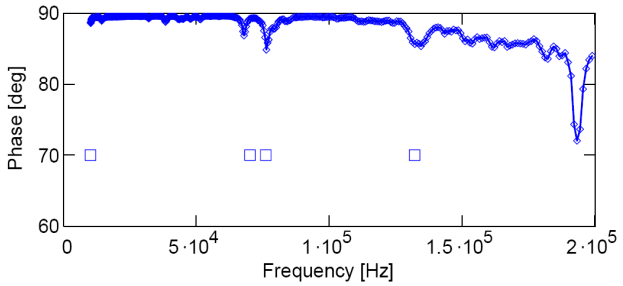

Figure 5. Admittance phase for motor 5. The points indicate frequencies of rotation (square = CW, circle = CCW).

Detailed measurements of the stall torque and frequency sensitivity were performed for selected strong rotations in motors 3 and 5. The stall torque is defined as the torque exerted on the rotor when the rotor is at rest. Assuming a frictional force proportional to rotational velocity $\dot{\theta}$, we have for the angular acceleration $d\dot{\theta}/dt$

$$\frac{d\dot{\theta}}{dt} = \frac{T_s}{J} - \frac{c}{J}\dot{\theta} \tag{5}$$

where T_s is the stall torque, J is the moment of inertia of the rotor, and c is a coefficient of friction. From this, we have

$$\dot{\theta}(t) = \frac{T_s}{c}\left(1 - e^{-ct/J}\right) = \dot{\theta}_m\left(1 - e^{-ct/J}\right) \tag{6}$$

where $\dot{\theta}_m$ is the steady-state angular velocity.

Figure 6 shows measurements of the angular velocity as a function of time when motor 3 is started from rest. The measurements fit the expression (6) and consequently the stall torque T_s can be extracted. The extracted values of T_s and the maximum angular velocity are shown in Table II.

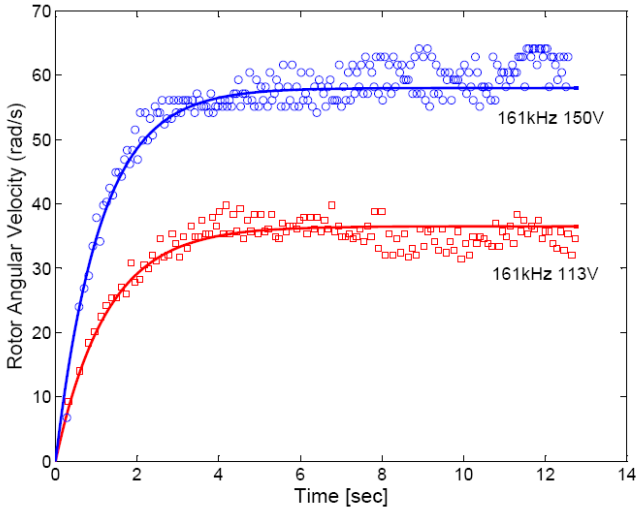

Figure 6. Rotational velocity of motor 3 as a function of time for two amplitudes of driving voltage.

TABLE II. PERFORMANCE PARAMETERS FOR PLEXIGLAS SPIRAL MOTORS,

Motor	Actuation Frequency	Drive voltage	RPM (max)	Stall Torque
3	161 kHz	150 V	570 rpm CW	2.8 μN·m
4	176 kHz	150 V	800 rpm CW	-
5	129 kHz	150 V	300 rpm CW	2.3 μN·m

In common with many designs of ultrasonic motors, good performance is obtained only for a narrow range of drive frequencies. Figure 7 and Figure 8 show the effect of drive frequency on steady-state rotor speed and torque for motor 3.

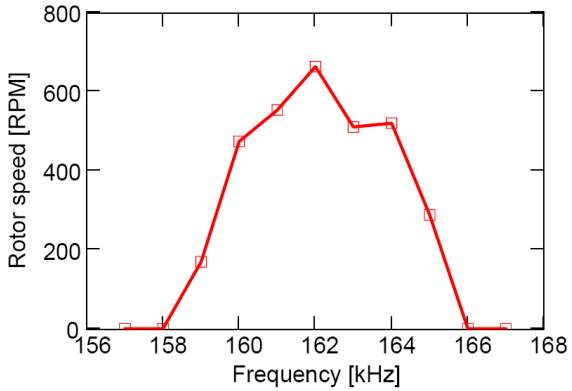

Figure 7. Effect of drive frequency on steady-state rotor speed (motor 3).

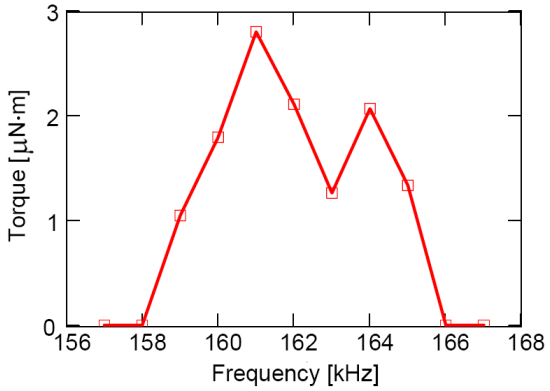

Figure 8. Effect of drive frequency on stall torque (motor 3)

Finally, we consider the effect of changing drive voltage. Figure 9 shows the effect of changing drive voltage on the steady-state rotor speed for motor 3. The rotor speed increases approximately linearly with drive voltage above a threshold at about 75 V. Approximately similar behavior is observed for the stall torque (not shown).

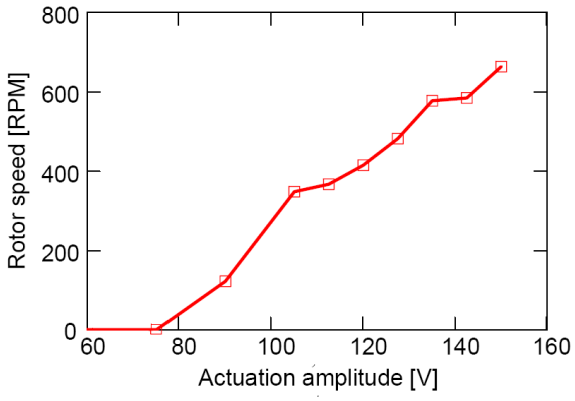

Figure 9. Effect of drive voltage on the steady-state rotational speed for motor 3 at 161 kHz.

Wajchman *et al.* [3] investigated in detail the dependence of stall torque and steady state rotational speed for one motor. They found that the stall torque was roughly proportional to preload and that the rotational speed was nearly independent of preload over the range investigated. For the rotor mass used in our experiments their motor would have a stall torque of about 14 μNm and a steady state speed of 170 RPM.

V. Double-Spiral Motor

In other work, we have noted that the boundary conditions imposed by the motor support can have a significant effect on the predicted rotation frequencies [5]. In order to avoid this problem, we have performed experiments on a symmetric double-spiral motor supported at the center between pieces of foam.

Measurements on the double spiral motor used lower drive voltages of about 35 V peak. In order to avoid missing frequencies which cause rotation, the generator frequency was swept slowly (~67 Hz/sec) under computer control while simultaneously measuring the rotational speed. These measurements were repeated several times and then averaged. Figure 10 shows both the data points from individual sweeps and the averaged speed. In these measurements the direction of rotation was recorded manually.

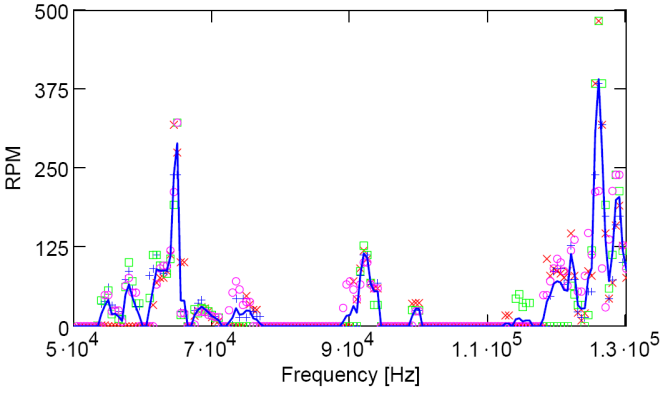

Figure 10. Rotation of double-spiral motor as a function of driving frequency.

A sweep performed in this way makes it easy to repeat measurements and to detect all frequencies that cause rotation. Additional sweeps beyond those presented in Figure 8 showed significant variability, with not all rotations observed consistently. The most robust rotations were at approximately 65 kHz (CW), 92 kHz (CCW) and 126 kHz (CCW and CW at closely spaced frequencies). This variability is not surprising since these motors are friction-driven and experience only small displacements at the stator tip, leading to a strong influence of local frictional variations and alignment. Comparison with simulations of the same structure showed partial agreement between predicted and measured frequencies of rotation. It is likely that better agreement between simulation and experiment will be obtained when the stators are fabricated more precisely.

Conclusions

We have adapted a previously reported spiral motor design for actuation by paired piezoelectric wafers. This design has the advantage of requiring a smaller volume of piezoelectric material and also a smaller reactive current for similar actuation amplitude. We have reported on the stall torque and steady-state rotational speed of this motor design.

Acknowledgment

The investigators would like to acknowledge support from the National Science Foundation under Grant CMS-0329880 entitled SENSORS: Collaborative Research: MEMS for Multi-Mode Civil Infrastructure Sensing, and by the Pennsylvania Infrastructure Technology Alliance.

References

[1] K. Nakamura, M. Kurosawa, and S. Ueha, "Design of a Hybrid Transducer Type Ultrasonic Motor," IEEE Transactions on Ultrasonics, Ferroelectrics, and Frequency Control **40**, 395-401 (1993).

[2] J. Tsujino, R. Suzuki, and H. Yasojima, "Load Characteristics of Ultrasonic Rotary Motor Using a Longitudinal-Torsional Vibration Converter," IEEE Ultrasonics Symposium 1996, pp. 377-382.

[3] D. Wajchman, K.-C. Liu, J. Friend, and L. Yeo, "An Ultrasonic Piezoelectric Motor Utilizing Axial-Torsional Coupling in a Pretwisted Non-Circular Cross-Sectioned Prismatic Beam," IEEE UFFC-55, p. 832 (2008).

[4] V. Giurgiutiu, "Lamb Wave Generation with Piezoelectric Wafer Active Sensors for Structural Health Monitoring," Smart Structures and Materials 2003: Smart Structures and Integrated Systems, 111.

[5] D.W. Greve and I.J. Oppenheim, "Modes and tip motions in ultrasonic motors using torsional/ longitudinal vibration," IEEE Ultrasonics Symposium 2009 (to be published).